AC motor impedance HF modeling for designing with windings variability

Arthur Piat, François Costa, Pierre-Etienne Lévy, Sébastien Serpaud, Sami Hlioui

AC motor impedance HF modeling for designing with windings variability

Arthur Piat[2,1]
[2]IRT Saint Exupéry Toulouse, France
[1]Université Paris-Saclay, ENS Paris-Saclay , CNRS, SATIE,
91190 Gif sur Yvette, France
arthur.piat@irt-saintexupery.com

Pierre-Etienne Lévy[1]
Université Paris-Saclay, ENS Paris-Saclay , CNRS, SATIE,
91190 Gif sur Yvette, France
pierre-etienne.levy@ens-paris-saclay.fr

Sami Hlioui[1,3]
[1]Université Paris-Saclay, ENS Paris-Saclay , CNRS, SATIE,
91190 Gif sur Yvette, France
[3]Cergy Paris-Seine University,
sami.hlioui@ens-paris-saclay.fr

François Costa[1,4]
[1]Université Paris-Saclay, ENS Paris-Saclay , CNRS, SATIE,
91190 Gif sur Yvette, France
[4]Université Paris Est Créteil,
94000 Créteil, France
francois.costa@ens-paris-saclay.fr

Sébastien Serpaud[2]
[2]IRT Saint Exupéry
31400 Toulouse, France
sebastien.serpaud@irt-saintexupery.com

***Abstract*—This paper presents a unified predictive modeling for common-mode (CM) and differential-mode (DM) impedance estimation of a Permanent Magnet Synchronous Motor (PMSM). This methodology combines 2D Finite Element modeling and generated lumped parameter circuit in Spice environment. It is then used to determine the consequences of design choices and evaluate the importance of controlling the winding process in the PMSM manufacturing. By doing so and by changing parts of the PMSM design, the overall high frequency response of the system with regards to input parameters can help in satisfying EMC high frequency constraints (between 1 kHz and 10 MHz).**

Keywords—Electromagnetic Compatibility (EMC), common-mode (CM), differential-mode (DM), electrical machine, HF modeling, finite element method

I. INTRODUCTION

In recent years, the trend in embedding electric systems in aircraft has allowed performance gains by reducing both the weight and the size of similar system using other sources of energy (hydraulic, pneumatic,…) [1]. Meanwhile, to further increase the power density of electrical systems, Wide-band gap semiconductor working at high switching frequency such as SiC and GaN became a key factor to reach higher thresholds of power transmission and reduce losses [2]. However, this increase of frequency and the faster switching time increases and enlarge the generated spectrum of Electromagnetic Interferences (EMI) [3]. As those perturbations are transmitted throughout the system, studies of propagation paths and dangers of such currents are well known and have been a focus of numerous experimental and measurements based articles [4]-[8].

Moreover, these currents can generate disturbances for neighboring systems [9] and must be limited with regard to various regulations [10]. In order to size passive filtering systems, a behavioral model could be created using series of measurements [11]-[14] however it requires to have a working prototype. Predictive modeling using Finite Element Methods (FEM) allowed predicting cable behavior [3] and this method was naturally used to evaluate electrical machine behavior at a broad spectrum of frequencies (few kHz up to 10 MHz) both in CM and DM [14]-[16] as well as estimating overvoltage within stator windings [17]-[19]. Likewise, an estimation of CM capacitance of a motor using probability density function showed variations in capacitance with various filling patterns [20]. However, the association of wire in parallel as well as wire turn's position relative to each other are not covered.

In this paper, we evaluate a methodology combining FEM and Spice circuit modeling to predict both CM and DM impedances on a frequency spectrum between 1 kHz up to 10 MHz. As it will be shown later, using this methodology with various windings, these tools give a better understanding of the variables needed to be adjusted to adapt the frequency spectrum of both CM and DM impedances.

II. MODELING AND HYPOTHESES

To study the impact of PMSM design variables, a model needs to be parametrized and computed in various configurations. A use case of a PMSM with a fixed slot form is selected. Only the winding is changed with regards to four parameters.

A. Number of turns in parallel

For a given power, a similar electrical machine can be created using different wires. Using wires in parallel, manufacturers can wind stators more easily than with a single and therefore more rigid wire, as it is assumed that thermal constraints will remain the same if the same copper surface is kept. A hypothesis is that parallel wires are considered at the same impedance at any frequency.

B. Dispersion in wire groups

Depending on the winding technique, wires in parallel may not stay in a perfectly stacked group, some wires may be mixed with other groups and will not form a perfect packing pattern. This difference induces a different level of interaction between each group (magnetic and capacitive) that need to be evaluated. The importance of such interactions in HF CM and DM modeling is yet to be quantified.

This paper is part of the OCEANE Project led by IRT Saint Exupéry, Toulouse (France), which is sponsored by AIRBUS, LIEBHERR, SAFRAN and the French National Research Agency (ANR) in collaboration with SATIE, TUD, DEEP, ICAM and LAPLACE.

C. *Order and position of wire groups in slots*

In a stator slot or winded rotor, the position of wire groups in a slot is heavily dependent on the manufacturing process, and this order can have significant consequences on partial discharge and voltage levels between turns [18]. Their consequences on CM and DM are yet to be quantified.

D. *Packing of wires within slots*

Wires, when placed in a slot, do not fill the form in perfect hexagonal or square patterns that can significantly change low frequency and high frequency behavior of the system [20]. This aspect will be partially addressed here.

A general workflow, presented in Fig. 1, allows considering all those parameters. The first step consists in defining a simplified geometry for the slot, only composed of lines (Illustrated by step 1 Fig. 1). This allows dividing the overall space and defining potential places for conductors. A mesh (different from FEM mesh) is refined until all conductors fit within a slot (Illustrated by step 2 Fig. 1). This allows changing between wire configurations (diameter and number). If a mesh allows for more than the needed number of wires, extra positions are randomly selected and removed (Illustrated by step 3 Fig. 1). This algorithm will fill any slot

Fig. 1. General workflow for winding randomization

volume with a hexagonal pattern. Afterwards, groups need to

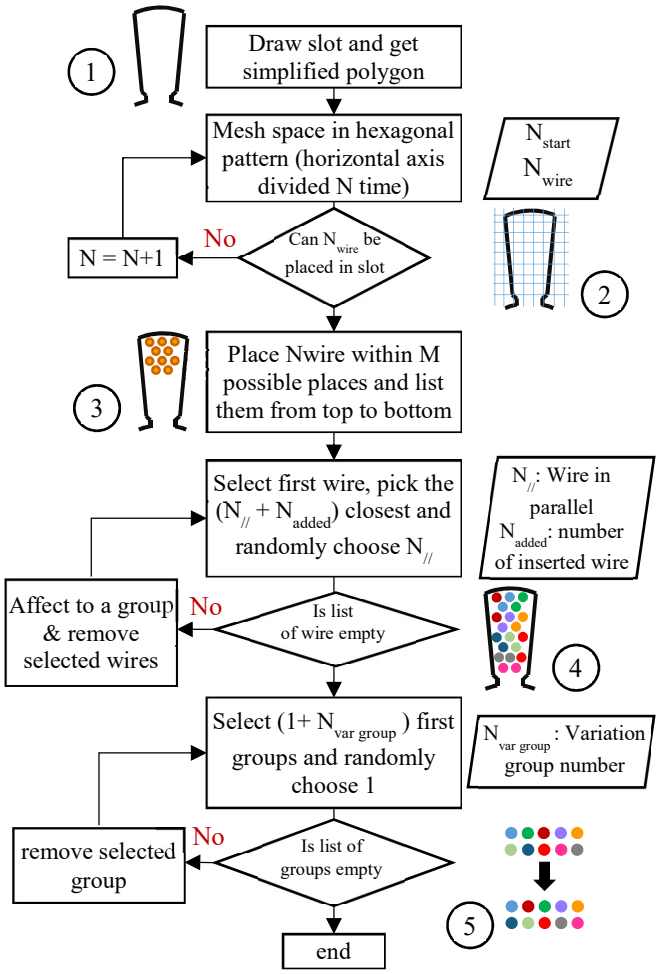

be defined, as wires in the same group are representing wires winded in parallel in the real motor. The variables $N_{var\ group}$ modify the way wires are grouped based on their relative distance: if $N_{var\ group}$ is equal to zero, only the closest wires are selected to be part of a group, if $N_{var\ group}$ is equal to the number of conductors, every conductor are suitable to be in any groups. For instance in step 4 Fig.1, $N_{var\ group}$ is equal to zero and groups of two wires are created, starting from the bottom center of the slot, the closest wire is grouped with its closest neighbor until all wires have a group.

Finally, N_{added} will randomly switch groups order depending on the given value. This allows for variability in association and organization but do not change conductors' position. As shown in step 5 Fig. 1, if N_{added} is equal to one, an inversion of group order can be observed randomly. This process was designed to maximize the repartition within slot, by creating such mesh, we are forcing all conductors to be separated in average by the maximal distance possible. Such filling strategy is not entirely representative to the configuration found in real motors as the manufacturing process can spatially move any wire and is not the same throughout the motor length [20] but allow for variation studies in winding. Once this workflow has modified the overall winding, a following workflow will allow extracting HF impedance similar to [14]-[16].

III. FE SIMULATIONS FOR IMPEDANCE EXTRACTION

The geometry defined by the algorithm will be used to generate three FE models: two magnetic analyses and an electrostatic one using FEMM [21]. As the 2D nature of these tools cannot replicate the complexity of real electrical machines, hypotheses were taken. Indeed, contrary to [16], end-windings considered as the studied motor is composed of almost two third of iron stack and one third of end-winding, inducing a significant amount of inductances in motor winding.

A. *Magnetic model for slot resistance and inductance*

A section of the motor is drawn with a pole. As this PMSM only have one phase by slot, only two windings are represented to form the global induction loop. All groups are excited one by one with a 1A current to extract self and mutual impedances.

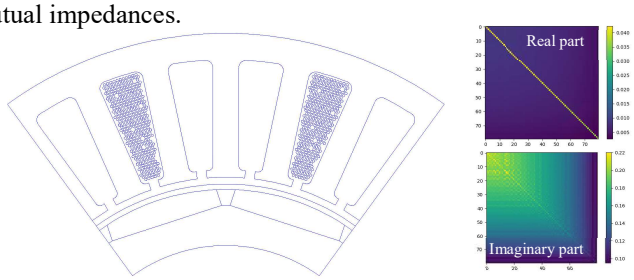

Fig. 2. Slot impedance characterization with FEMM

For a given configuration of winding, all conductors in the same group are considered in parallel therefore the current is applied to all conductors leading to an overall impedance. By dividing the voltage drop, noted ΔV, by the total current I_i flowing thought conductors in group i, resistances R and mutual- as well as self-inductances L matrices are computed.

$$L_{ij} = imag(\Delta V_j / I_i)/w \quad (1)$$

$$R_{ij} = real(\Delta V_j / I_i) \quad (2)$$

i: Group with 1A imposed current, w=2πf

For this simulation, insulation on the wire and in the slot is not represented as they behave very similarly to the air. Meshing is narrowed within each conductor with regards to skin depth to extract coherent values. Magnetic simulations are performed up to 10MHz, refining the mesh on wire circumferences result in more computationally intensive simulations at high frequency and in some cases instability in FEMM software. Therefore, simulations do not exceed 10MHz. Finally, to consider the machine magnetization stack created by magnets, a simulation is performed beforehand without any current. The magnetic circuit characteristics are imported afterwards using the frozen permeability feature of FEMM software.

B. *Capacitive model for turn-to-turn and turn-to-ground*

Regarding capacitive computation, the process is similar to inductance and resistance estimation. All conductors in one group have their surfaces excited at 1V, noted V_i, in an electrostatic simulation while all others, as well as the slot border, are fixed at 0 V. Capacitance's matrices C are therefore computed dividing surface charges q_j on conductor j by V_i as shown on equation (3).

$$C_{ij} = q_j / V_i \tag{3}$$

i: Group with 1 V imposed excitation

It is to be noted that in case of i=j, the capacitance is in fact $C_{i\text{-ground}}$ meaning the capacitance between the group i and the slot surface.

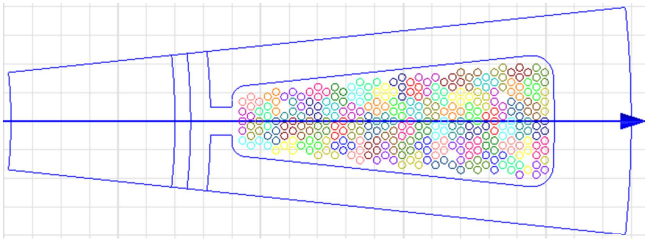

Fig. 3. Depiction of capacitive model with no enamel and insulating paper, featuring wire groups

C. *Magnetic model for end-winding impedance*

The total length of the motor studied is composed of one third of end-winding. Consequently an end-winding model was developed. However, using 2D FEM models, strong hypotheses need to be taken. The chosen approach uses an axisymmetric model, all conductors are kept in the same position as within the slot (see Fig. 4.) and the distance to the revolution axis is half the distance between the two slots used by one coil, creating half a circle to create a circularly ideal end-windings. Coupling inductances between different phases are likewise considered negligible. Finally, inductances and resistances are computed similarly to their slot counterpart using equation (1) and (2).

For the following results, the values chosen are: copper electrical conductivity, 58 MS/m and relative permittivity equal to 1. M-36 Steel FEMM default material with a relative permittivity of 2.164. Wire insulation and slot insulation layer have both an electrical conductivity of 0 MS/m (like air) but a relative permittivity of 5.

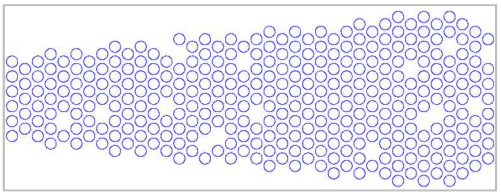

Fig. 4. End-winding model geometry using asymetric simulation

IV. SPICE CIRCUIT GENERATION

All FEM simulations need to be integrated in an overall circuit to allow CM and DM impedances characterization. The electric model corresponding to one slot of Fig. 5. with associated nomenclature of Table I. are presented for a motor with a single phase by slot. Two main repeating units compose this circuit:

TABLE I. NOMENCLATURE USED FOR LUMPED PARAMETERS

Type	Type of element used: **L** for inductances, **R**, **K** ,**V, C** for resistance, coupling coefficient, real impedance coupled generators and capacitances respectively
Position	Position indices in loop: **s** for slot, **a** for air
Direction	Direction: **a** for first half if loop, **r** for return
Number	Number of completed loop (stating at 0) If only a number is given: self-property If two numbers are given: coupled property
Examples: **Csa0_5**: Capacitance in first slot between wires 0 and 5 **Lar8**: self-inductance of wire 8 in return end-winding **Vaa6**: Real impedance coupled generators of group 6 in first end-winding	

A. *Slot model with capacitive and inductive coupling*

Ls and Rs components are respectively filled using R_{ii} and L_{ii} from (1) and (2), similarly Cs is derived from (3). As one coil will go through two slots, this part needs to be repeated twice to get the desired behavior (Lsa - Lsr, Rsa-Rsr and Csa-Csr). Finally, as this repeating unit is used for each turn in the electrical motor slot, mutual inductances between each group

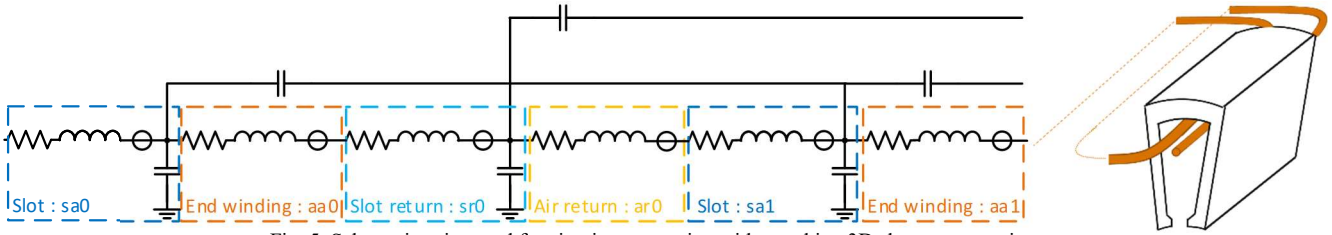

Fig. 5. Schematic spice used for circuit construction with matching 3D slot representation

are implemented using equation (4) as Spice solver uses coupling factors and not mutual impedances.

$$k_{ij} = L_{ij} / \sqrt{L_{jj} \cdot L_{ii}} \quad (4)$$

These coupling coefficients are named Ksa, Ksr, Kaa and Kar matching the previous notation.

B. Coupled real impedance generators

To add the real part of the coupled impedance, no passive components exist apart from coupling factor in inductances. The real part of coupled impedances can be represented in using behavioral voltage sources in Spice simulator. The schematic described [16] is not easily implementable in previous developed work therefore the following method was preferred:

$$V_i = \sum I_j . R_{ij} \ , \ \forall i \neq j \quad (5)$$

One behavioral voltage source is used for each wire but the expression depends on the current within other groups. This source acts very similarly to coupling coefficient for inductances and will "transfer" energy from one wire group to other groups. Similarly, coupling coefficient between inductances are placed for each conductor at every turn of the winding. The nomenclature adopted is Vsa, Vsr, Vaa and Var.

C. End winding model

Regarding the end winding, only the magnetic model was developed. Therefore, only a resistor and an inductance are used for both sides of the electrical machine (Raa, Rar and Laa, Lar respectively) as well as coupling coefficient (Kaa and Kar).

A resulting circuit with 4n(n+3) components is generated for each frequency point simulated and solved by LTSpice, n being the number of turns. Capacitive couplings are considered constant at each frequency while resistance and inductance are highly impacted by skin and proximity effect. FEMM magnetic models are simulated at various frequencies and matrices are linearly interpolated to obtain in-between values. Laplace voltage-controlled generators were investigated similarly to [16] but due to the extensive number of expressions needed for an eighty-turn electrical machine, the previous approach was preferred.

Within these netlist, a voltage generator is placed either between ground and sa0 (node at the beginning of the coil) or between sa0 and arN (N being the number of turns) for respectively Common-mode and Differential-mode impedance characterization. Combining these values and matching measurement on existing motor will allow validating the overall approach, similarly to [14]-[16].

V. Studied Configurations and HF Trade-off

Three configurations are studied in this paper, depicted in Table II. The aim is to compare three electrical machines considered equivalent from a mechanical standpoint but with different types of winding. The chosen enamel thickness matches the average IEC 06317 grade 2, apart from S3 which is an estimated value to keep the same copper surface for all tested values. All these configurations are simulated with tools described before, allowing plotting both CM and DM impedances.

The following comparisons are based on a single coil and not on a full motor. On Fig. 5, Table II configurations are simulated, configuration S1 is plotted in blue, S2 in orange and S3 in red. Some lumped parameters are computed in Table III for comparison, they are described hereunder.

TABLE II. Studied Electrical Machine Configurations

Reference	Design variables		
	Winding copper diameter	*Enamel thickness*	*Wire in parallel*
S1	1.0 mm	0.08 mm	1
S2	0.5 mm	0.055 mm	4
S3	0.25 mm	0.041 mm	16

TABLE III. Equivalent Lumped Parameters Level for HF Models

Reference	Estimated lumped parameters		
	CM capacitance	*DM inductance*	*AC resistance* (1MHz)*
S1	82.8 pF	3.11 mH	44.8 Ω
S2	137 pF	3.09 mH	39.3 Ω
S3	216 pF	3.07 mH	38.7 Ω

*defined in Section V, Subsection C

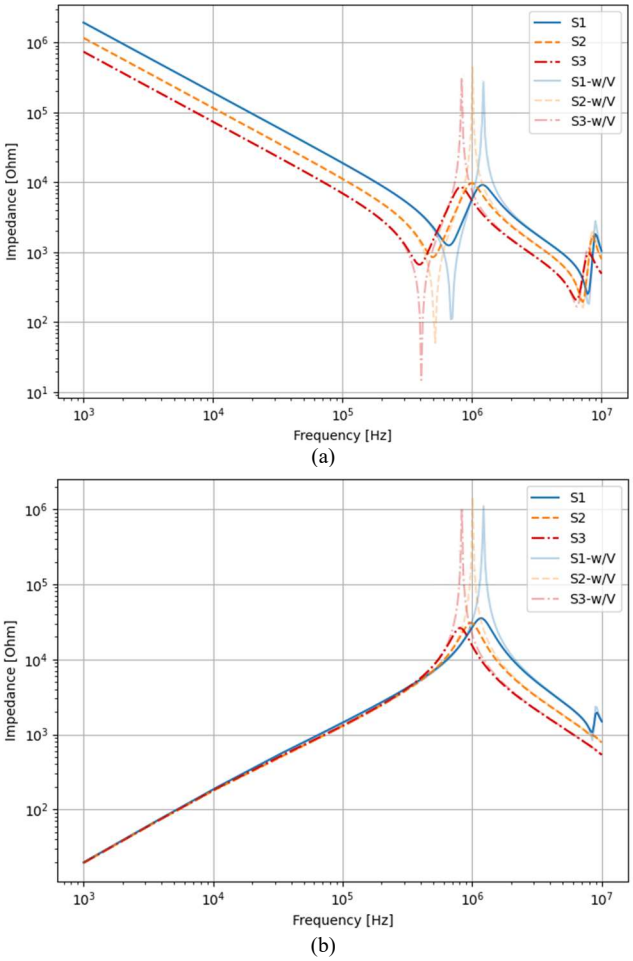

Fig. 6. Common-mode (a) and Differential-mode (b) impedance of a simulated 80 turn coil within a stator using different winding

A. Common mode impedance

The common mode capacitance is the low frequency capacitance that can be seen on Fig. 5 (a). It is computed with either Spice simulation or using capacitance matrix trace. As more parallel conductors are used, more energy is stored between wires and the slot. This can be explained as the small wire tend to fill more the space around the slot edge, resulting in an increase of the capacitance between groups and the slot surface. Moreover, the enamel thickness does not decrease proportionally to the copper diameter, resulting in a bigger proportion of material with a high relative permittivity.

B. Differential mode inductance

Similarly to CM capacitance, DM inductances are estimated using the first part of curves on Fig. 6 (b). However, computing it from matrices can be difficult as coupled inductances impact the slope at the first order. This value does not vary significantly from configuration S1 to S3.

C. AC resistance of coil

AC resistance is estimated as the sum of all resistances in series in the circuit Fig. 6, or more simply the trace of matrix R, equation (2) at a given frequency. As this value is highly frequency dependents, a comparison between configurations is performed at 1 MHz. As this frequency, both skin and proximity effect highly impact the overall value. By computing the trace of the matrix resistance, it appears as if loss remains similar for every configuration. This result is counterintuitive to the fact that Litz wire reduces losses [22], but these observations are made at the motor working frequency and not at high frequency.

D. Real impedance coupled voltage generators

In preliminary result, the real part of coupled was neglected similarly to [14] and no voltage controlled were used. As seen on Fig. 6, such circuit presented resonances with no damping (see S3-w/V compared to S3). According to [14][15], the damping was not present in the curves obtained as no dielectric and iron losses were modeled. However [16] have significant damping due to coupled real impedances but do not use any dielectric losses. Both authors in [14] and [23] noted a significant difference between their models and impedance measurements in particular on damping. No conclusion can be drawn to this question in the current study and further work is needed to conclude on the need to combine those aspects. By comparing the curve from S1 to S3, not a significant difference in damping can be observed between each configuration. The origin of such losses can be linked to induced current within other wires, coupled with proximity and skin effect. However as the frequency increases, the damping on resonances returns to the level of simulations without voltage source.

E. General remarks on impedance curves and resonances

Regarding common mode, the low frequency capacitance seen on the various curves is driven by the capacitances of wires to slots, the first resonance is due linked to the line inductance (DM inductance in Table III), as this inductance remains the same for all configurations, the first resonance is displaced at lower frequency whenever the CM capacitance is increased. The second resonance on CM impedance is between the line inductances and turn-to-turn: as a difference in potential appears between each turn, a new association of capacitance is excited combining turn-to turn and turn-to-slot capacitances. It is believed that following resonances are the consequences of the transmission line behavior of the system between the non-linear inductances of wires and all capacitances. The DM inductance computed Table III drives DM impedances for the most part, skin and proximity effect change the value of self and mutual inductance, this results in a slight decline from the expected 20dB/decade slope, up until the first resonance with turn-to-turn capacitances change the behavior of the curve. Resonance frequencies match the CM impedance curve, resulting in similar behavior in both curves after the second and first resonance from CM and DM impedances respectively, implying that turn-to-turn capacitance is the main factor determining the first DM impedance resonance frequency in this winding configuration. All these aspects need to be validated on prototypes for further discussion.

CONCLUSION

In this paper, HF identification and simulation methodologies for various PMSM winding types were developed and tested. Increasing the number of wires in parallel for a given configuration of slots and turns number have a high risk of decreasing the resonances frequency mainly driven by wire to slot capacitance. These phenomena will directly influence the system response to various regulations [10]. Further work is needed: dielectric losses need to be integrated to represent more accurately the resonance amplitudes and a capacitive model of end winding will allow for a more accurate representation of impedance value after the first resonances. Meanwhile, estimating the impact of such behavior on the overall power drive and filtering systems will enlighten which trade-off needs to be made to improve global performances, with regard to regulation and system constraints. The robustness of such trade-off needs to be tested by introducing uncertainties in the winding that will represent the variations induced by fabrication processes. Finally, real life measurements and experiments are planned to validate our approaches on multiple demonstrators.

REFERENCES

[1] R. Berger, M. Nazukin, N. Sachdeva and N. Martinez, “Think: Act Aircraft Electrical Propulsion - The Next Chapter of Aviation ?” Roland Berger LTD, 2017

[2] H. H. Sathler, “Optimization of GaN-based Series-Parallel Multilevel Three-Phase Inverter for Aircraft applications”. Diss. Université Paris-Saclay, 2021.

[3] V. Dos Santos, “Modélisation des émissions conduites de mode commun d'une chaîne électromécanique: Optimisation paramétrique de l'ensemble convertisseur filtres sous contraintes CEM”. Diss. Toulouse, INPT, 2019.

[4] T. Hadden et al., “A Review of Shaft Voltages and Bearing Currents in EV and HEV Motors,” in IECON 2016 - 42nd Annual Conference of the IEEE Industrial Electronics Society, Oct. 2016, pp. 1578–1583. doi: 10.1109/IECON.2016.7793357.

[5] M. J. Costello, “Shaft voltages and rotating machinery,” IEEE Trans. Ind. Appl., vol. 29, no. 2, pp. 419–426, Mar. 1993, doi: 10.1109/28.216553.

[6] T. Plazenet, T. Boileau, C. Caironi, and B. Nahid-Mobarakeh, “A Comprehensive Study on Shaft Voltages and Bearing Currents in Rotating Machines,” IEEE Trans. Ind. Appl., vol. 54, no. 4, pp. 3749–3759, Jul. 2018, doi: 10.1109/TIA.2018.2818663.

[7] M. Asefi and J. Nazarzadeh, “Survey on high-frequency models of PWM electric drives for shaft voltage and bearing current analysis,”

IET Electr. Syst. Transp., vol. 7, no. 3, pp. 179–189, Sep. 2017, doi: 10.1049/iet-est.2016.0051.

[8] U. T. Shami and H. Akagi, “Identification and Discussion of the Origin of a Shaft End-to-End Voltage in an Inverter-Driven Motor,” IEEE Trans. Power Electron., vol. 25, no. 6, pp. 1615–1625, Jun. 2010, doi: 10.1109/TPEL.2009.2039582.

[9] Morgan, D., and B. Mulhall. "A Handbook for EMC Testing and Measurement." Measurement Science and Technology 6.5 (1995): 600.

[10] Mariscotti, Andrea, and Leonardo Sandrolini. "Review of models and measurement methods for compliance of electromagnetic emissions of electric machines and drives." *ACTA IMEKO* (2021).

[11] D. Zhao, K. Shen, W. Liu, L. Lang and P. Liang, "A Measurement-Based Wide-Frequency Model for Aircraft Wound-Rotor Synchronous Machine," in IEEE Transactions on Magnetics, vol. 55, no. 7, pp. 1-8, July 2019, Art no. 8105408, doi: 10.1109/TMAG.2019.2900616.

[12] Kohji Maki, Hiroki Funato and Liang Shao, "Motor modeling for EMC simulation by 3-D electromagnetic field analysis," 2009 IEEE International Electric Machines and Drives Conference, 2009, pp. 103-108, doi: 10.1109/IEMDC.2009.5075190.

[13] M. A. Gries and B. Mirafzal, "Permanent Magnet Motor-Drive Frequency Response Characterization for Transient Phenomena and Conducted EMI Analysis," IEEE APEC 2008 (2008) pp.1767-1775.

[14] N. Boucenna, “Contribution à la modélisation en compatibilité électromagnétique des machines électriques triphasées”. Diss. École normale supérieure de Cachan-ENS Cachan, 20

[15] N. Boucenna, F. Costa, S. Hlioui and B. Revol, "Strategy for Predictive Modeling of the Common-Mode Impedance of the Stator Coils in AC Machines," in IEEE Transactions on Industrial Electronics, vol. 63, no. 12, pp. 7360-7371, Dec. 2016, doi: 10.1109/TIE.2016.2594052.

[16] J. E. Ruiz-Sarrió, F. Chauvicourt, J. Gyselinck and C. Martis, "High-Frequency Modelling of Electrical Machine Windings Using Numerical Methods," 2021 IEEE International Electric Machines & Drives Conference (IEMDC), 2021, pp. 1-7, doi: 10.1109/IEMDC47953.2021.9449561.

[17] Pastura, Marco & Nuzzo, Stefano & Immovilli, Fabio & Toscani, Andrea & Rumi, Alberto & Cavallini, Andrea & Franceschini, Giovanni & Barater, Davide. (2021). Partial Discharges in Electrical Machines for the More Electric Aircraft—Part I: A Comprehensive Modeling Tool for the Characterization of Electric Drives Based on Fast Switching Semiconductors. IEEE Access. PP. 1-1. 10.1109/ACCESS.2021.3058083.

[18] V. Mihaila, “Nouvelle Conception des bobinages statoriques des machines à courant alternatif pour réduire les effets négatifs des dV/dt”. Diss. Artois, 2011.

[19] V. Mihaila, S. Duchesne and D. Roger, "A simulation method to predict the turn-to-turn voltage spikes in a PWM fed motor winding," in *IEEE Transactions on Dielectrics and Electrical Insulation*, vol. 18, no. 5, pp. 1609-1615, October 2011, doi: 10.1109/TDEI.2011.6032831.

[20] A. Hoffmann, B. Knebusch, J. O. Stockbrügger, J. Dittmann and B. Ponick, "High-Frequency Analysis of Electrical Machines Using Probability Density Functions for an Automated Conductor Placement of Random-Wound Windings," *2021 IEEE International Electric Machines & Drives Conference (IEMDC)*, 2021, pp. 1-7, doi: 10.1109/IEMDC47953.2021.9449557.

[21] D. Meeker, “Finite element method magnetics,” FEMM, vol. 4, p. 161, 2020.

[22] M. S. C. Pechlivanidou and A. G. Kladas, "Litz Wire Strand Shape Impact Analysis on AC Losses of High-Speed Permanent Magnet Synchronous Motors," *2021 IEEE Workshop on Electrical Machines Design, Control and Diagnosis (WEMDCD)*, 2021, pp. 95-100, doi: 10.1109/WEMDCD51469.2021.9425656.

[23] Ruiz-Sarrio, Jose E., et al. "Impedance Modelling Oriented Towards the Early Prediction of High-Frequency Response for Permanent Magnet Synchronous Machines." *IEEE Transactions on Industrial Electronics* (2022).